Am J Nucl Med Mol Imaging 2019;9(4):193-202
www.ajnmmi.us /ISSN:2160-8407/ajnmmi0098130

Original Article

Renal statistical map for positron emission tomography with [O-15] water

Mahabubur Rahman[1,4,5], Hiroshi Watabe[1], Miho Shidahara[2], Shoichi Watanuki[3], Manabu Tashiro[3], Takefumi Mori[6], Sadayoshi Ito[7], Yusuke Ohsaki[8]

[1]Division of Radiation Protection and Safety Control, Cyclotron and Radioisotope Center (CYRIC), Graduate School of Biomedical Engineering, [2]Division of Applied Quantum Medical Engineering, Department of Quantum Science and Energy Engineering, Graduate School of Engineering, [3]Division of Cyclotron Nuclear Medicine, CYRIC, Tohoku University, Aoba-6-3, Aramaki, Aoba-ku, Sendai-shi, Miyagi-ken 980-0845, Japan; [4]Bangladesh Atomic Energy Commission, E-12/A, Shahid Shahabuddin Shorok, Dhaka 1207, Bangladesh; [5]Bangladesh Atomic Energy Regulatory Authority, E-12/A, Shahid Shahabuddin Shorok, Dhaka 1207, Bangladesh; [6]Division of Nephrology and Endocrinology, Tohoku Medical and Pharmaceutical University, 1-15-1 Fukumuro, Miyagion-ku, Sendai 983-8536, Japan; [7]Division of Nephrology, Endocrinology and Vascular Medicine, Tohoku University Hospital, [8]Division of Integrated Renal Replacement Therapy, Tohoku University Graduate School of Medicine, 1-1 Seiryo-cho, Aoba-ku, Sendai 980-8574, Japan

Received June 7, 2019; Accepted July 8, 2019; Epub August 15, 2019; Published August 30, 2019

Abstract: Image statistics are frequently used for functional and molecular imaging research in which images from a patient group with a specific diagnosis are compared with images from a healthy control group who have been matched for demographic variables. The success of image statistics for brain imaging has encouraged us to develop a method for obtaining volumetrically normalized kidney to perform image statistics so that we can locally visualize the statistical significant difference comparing voxel by voxel between certain groups in terms kidney blood flow kinetic parameters. For the development of this evolutionary process, we first volumetrically normalized all subjects, which include healthy control (HC) and chronic renal failure (CRF) patients, ^{15}O water PET image with respect to one HC subject's MRI image using affine transformation. Then ^{15}O kinetic parametric images of normalized kidneys were obtained through the basis function method. Finally, the statistical map of these parametric images was produced using the threshold-free cluster enhancement based permutation method. Kinetic parameters of kidney namely, uptake rate constant (K_1), clearance rate constant (k_2) and blood volume (V_a), were found to be notably lower in CRF than those of in HC and k_2 parameter was found to be more stable compared to K_1 and V_a. The statistical map of these parametric images allowed us to visualize local significant differences statistically ($P<0.05$) between HC and CRF groups. Though PET and MRI techniques have enormous potentiality for functional and molecular imaging of kidney, these are, at best, in experimental level. It is speculated that statistical mapping of kidney could play a significant role in the successful implementation of functional and molecular kidney imaging. However, more research involving a larger sample size and improved normalization technique will be needed for the robustness of the process.

Keywords: Statistical map, volumetric normalization, kidney imaging, PET, [O-15] water

Introduction

Molecular imaging is playing a vital role in research, diagnosis and management of kidney disease. Noninvasive imaging modalities like positron emission tomography (PET), single photon emission computed tomography (SPECT), magnetic resonance imaging (MRI) and ultrasound imaging (UI) are popular for obtaining the molecular image of kidney. Among them SPECT has widely been used clinically to determine the symmetry of the disease and provide information on kidney size and overall perfusion [1]. However, intra-renal flow distribution cannot be determined by SPECT. Fortunately, tomographic spatial resolution of PET, which is similar to the thickness of the renal cortex, along with its efficient attenuation correction, scatter correction and image reconstruction process makes it an excellent imaging modality not only

for straightforward quantification of renal blood flow and glomerular filtration rate but also for quantitative imaging of molecular targets [2]. In the physiology of the kidney, renal blood flow (RBF) is the volume of blood delivered to the kidneys per unit time. In humans, the kidneys together receive roughly 25% of cardiac output, amounting to 1.1 L/min in a 70-kg adult male. Reduction in RBF is commonly detected in patients with ischemic acute kidney injury (AKI), renal artery stenosis, obstructive nephropathy, or decreased mean arterial blood pressure [3]. RBF measurement with PET offers prospective applications in renovascular disease, in rejection or acute tubular necrosis of transplanted organs, in drug-induced nephropathies, ureteral obstruction, before and after revascularization, and before and after placement of ureteral stents [2].

Parametric images of kidney with $H_2{}^{15}O$ and PET enabling clinicians to study intra-organ differences in perfusion as opposed to overall organ blood flow. Using the parametric map mean perfusion of a specific tissue can be determined by averaging all voxels within that tissue. Therefore, such maps could enable the study of differential perfusion between cortex and medulla in kidney disease patients and to identify ischemic and hyperemic areas within the kidney. Mapping of local blood flow with $H_2{}^{15}O$ and PET has been validated in kidney and in other organs [4-8], suggesting $H_2{}^{15}O$ is the most suitable radiotracer for measuring local blood flow with PET. Furthermore, volumetric normalization of an organ, which is to bring that organ volume obtained from different individuals in a common reference space called template, has become a necessary part of structural and functional data analysis. Such normalization can be used to perform image statistics over a sample of subjects in this reference space within which standardized anatomic labeling can also be implemented across subjects, studies and laboratories [9]. Therefore, volumetric normalization of parametric images of kidney could enhance the study performance of intra-rogan differences since such approach has successfully been used in brain and cardiac blood flow imaging both in research and clinical practice.

Image statistics so-called statistical mapping has widely been used in studies in which images from a patient group with a specific diagnosis are compared with images from a healthy control group who have been matched for demographic variables. This comparison between groups is performed voxel by voxel for testing the differences between the means of the two sets of data while taking the variance within groups into account. Image statistics also enable statistical comparison between different subgroups of patients. Furthermore, by quantifying each voxel using standardized scale correlation between regional function patterns among samples of patients and the severity of specific symptoms can be obtained. Following several stages of image preprocessing including smoothing, realignment and volumetric normalization image statistics is compiled and evaluated to find significant foci in a standardized anatomical space [10]. Automatic analysis methods [11-13] using image statistics and volumetric normalization have already been incorporated into the clinical routine within nuclear medicine and in other medical fields of medical knowledge, specifically in nuclear cardiology [14]. However, this type of analysis continues to be minimally explored in clinical practice within nephrology [10].

We have been motivated by the success of image statistics of brain imaging to develop a method for obtaining volumetrically normalized kidney to perform image statistics so that we can locally visualize the statistical significant difference comparing voxel by voxel between certain groups in terms of kinetic parameters of kidney blood flow.

Materials and methods

Subjects

Retrospective image data from 2011 to 2015 of ten human subjects which include two females were studied. Among them, four were clinically diagnosed as chronic renal failure (CRF) patients and six were healthy controls (HC). The average age, height and weight of the HC subjects were (40±6) years, (171±3) cm and (82±11) kg, respectively and those for CRF were (58±10) year, (159±12) cm and (66±22) kg, respectively.

Image acquisition

PET scans using $H_2{}^{15}O$ radioisotope were performed on HC and CRF subjects under rest con-

dition. Among them, only two HC underwent three dimensional (3D)-PET scan in 2015 while the rest underwent two dimensional (2D)-PET scan from 2011 to 2013. 2D mode PET scans were performed using a Shimadzu SET-2400W scanner [15] and 3D mode PET scans were performed using a Shimadzu Eminence (SET-3000 B) scanner [16]. The average injected activity for 3D and 2D mode PET scan were (84±8) MBq and (607±83) MBq, respectively.

For 3D scan mode, scan protocol for one subject was 36 frames, 4 min (6 sec × 5 frames, 3 sec × 20 frames, 6 sec × 5 frames, 20 sec × 6 frames) and that for the other subject was 37 frames, 5 min (6 sec × 5 frames, 3 sec × 20 frames, 6 sec × 5 frames, 20 sec × 7 frames). Images were reconstructed using 'Dynamic RAMLA (Row-Action Maximum Likelihood Algorithm) [17], (DRAMA)'-3D [18] where the reconstruction parameters, iteration and subset were 1 and 128, respectively and the image matrix and voxel size were 128 × 128 × 79 and 4 × 4 × 3.25 mm^3, respectively.

For 2D scan mode, scan protocol for two subjects were 50 frames, 5 min (3 sec × 20 frames, 6 sec × 20 frames, 12 sec × 10 frames) and that for the rest subjects were 36 frames, 4 min (6 sec × 5 frames, 3 sec × 20 frames, 6 sec x 5 frames, 20 sec × 6 frames). Images were reconstructed using 2D-Ordered Subsets Expectation Maximization (OSEM) [19] where the reconstruction parameters, iteration and subset were 2 and 16, respectively and the image matrix and voxel size were 128 × 128 × 63 and 4 × 4 × 3.125 mm^3, respectively.

MRI for only one HC subject was produced with GE Signa™ HDxt 1.5T magnetic resonance scanner. The T1-weighted MR image Sequence was LAVA-FLEX where the matrix and voxel size were 512 × 512 × 112 and 0.684 × 0.684 × 2.5 mm^3, respectively. This HC subject's 3D PET image and MR image were used as the reference image for the volumetric normalization process.

Statistical parametric image processing

Basis function method (BFM): The BFM has been used to estimate kinetic parameters of blood flow at voxel level for organs and eventually generating the parametric images. We embraced the concept of the BFM and implemented it to generate parametric images of blood flow namely, uptake rate constant K_1 as ml/min/g, clearance rate constant k_2 as min^{-1} and the activity concentration in the arterial vascular space V_a as ml/ml. The BFM used the following kinetic model for $H_2{}^{15}O$ based on a single-tissue compartment model:

$$C(t)=V_a \bullet A(t) + k_1 \bullet A(t) * e^{-k_2 t}$$

Where, C(t) is the radioactivity concentration in a voxel of PET image; A(t) is the arterial input function; * indicates the convolution integral and K_1 (ml/min/g), k_2 (min^{-1}) and V_a (ml/ml) are the parameters of interest.

The BFM used in this study is illustrated in **Figure 1** where the range of k_2 is set to 0.34 (decay constant of ^{15}O) $<k_2<=24$ min^{-1} and 300 discrete basis functions were generated.

The aorta input function was obtained from the image-driven noninvasive profile fitting method [26].

Working procedure: We made averaged image of each subject's PET dynamic image over time frames. Then right and left kidneys were three-dimensionally cropped from the MR image, averaged and dynamic PET images.Using the FMRIB's Linear Image Registration Tools (FLIRT) [27, 28]- v6 of FSL-5 software the cropped average PET image of the kidney (CAPIK) was then registered on the cropped MR image of the kidney (CMIK). The transformation matrix obtained from the registration process was then applied to the cropped dynamic PET image of the kidney (CDPIK) to obtain registered CDPIK in MR coordinate. In this way, using the affine transformation right and left kidney of all subjects were separately normalized to the reference subject's MR image right and left kidney, respectively. The BFM was applied to each subject's normalized kidney image to get its parametric images. This process is repeated for all subjects. The statistical images were then created using two-sample unpaired t-test along with threshold-free cluster enhancement (TFCE) [29, 30] in permutation methods (also known as randomization methods) [31] of FSL to locally visualize the statistical significance ($P<0.05$) between HC & CRF. The flow chart of the parametric image processing is shown in **Figure 2**.

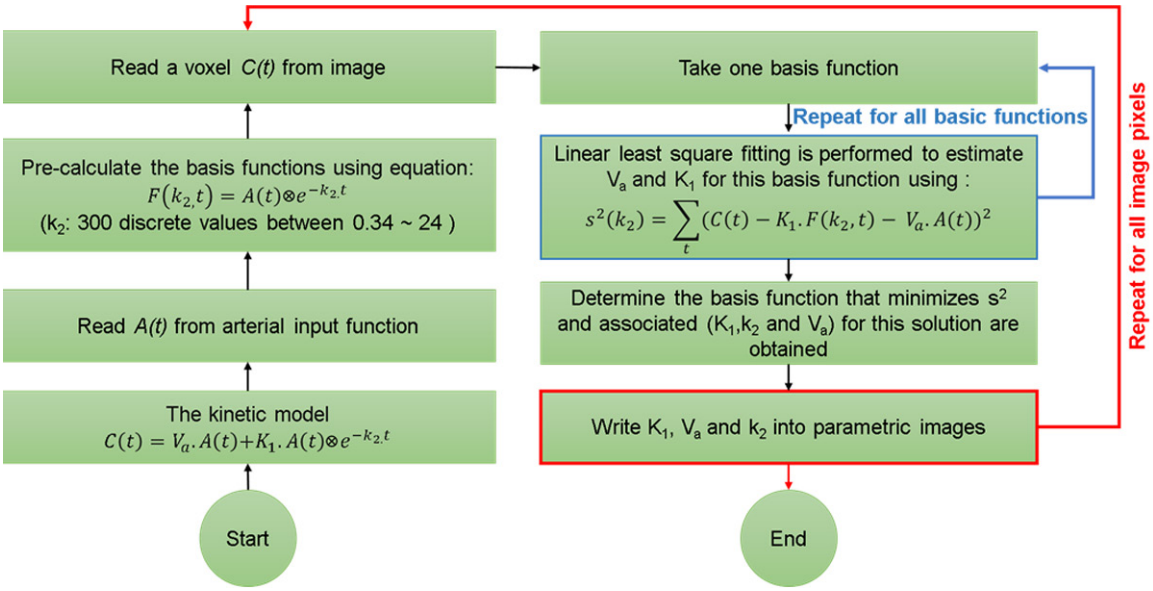

Figure 1. Basis Function Method (BFM) workflow.

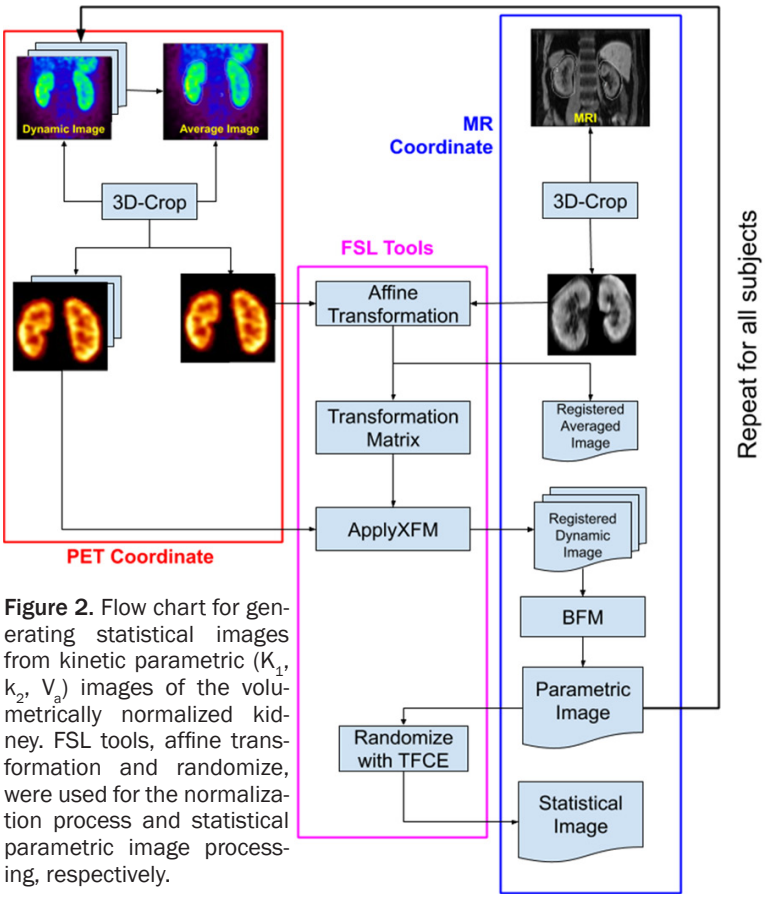

Figure 2. Flow chart for generating statistical images from kinetic parametric (K_1, k_2, V_a) images of the volumetrically normalized kidney. FSL tools, affine transformation and randomize, were used for the normalization process and statistical parametric image processing, respectively.

Reference subject's 3D-PET image (CAPIK) was directly registered to its CMIK (**Figure 3A**) but other subjects' CAPIK were first registered to reference subject's 3D-PET image (CAPIK) then registered to reference subject's CMIK (**Figure 3B**). Since 3D mode PET scan produced better quality image compared to the 2D mode PET scan, intermediate PET_{Otr} to PET_{Ref} registration within the process (b) (**Figure 3B**) help us to obtain better registration in MR space even for CRF subjects.

Results

Parametric images generated from volumetrically normalized kidney images using the BFM are shown in **Figure 4**. The K_1, k_2 and V_a values ranges from 0 ml/min/g to 4 ml/min/g, from 0/min to 8/min and from 0 ml/ml to 0.5 ml/ml, respectively.

Box plots (**Figure 5**) are showing that K_1, k_2 and V_a are notably lower in CRF than those of in HC and k_2 parameter is more stable compared to K_1 and V_a, because K_1 and V_a are highly affected by tissue mixture and partial volume effect whereas k_2 is not [5]. Box

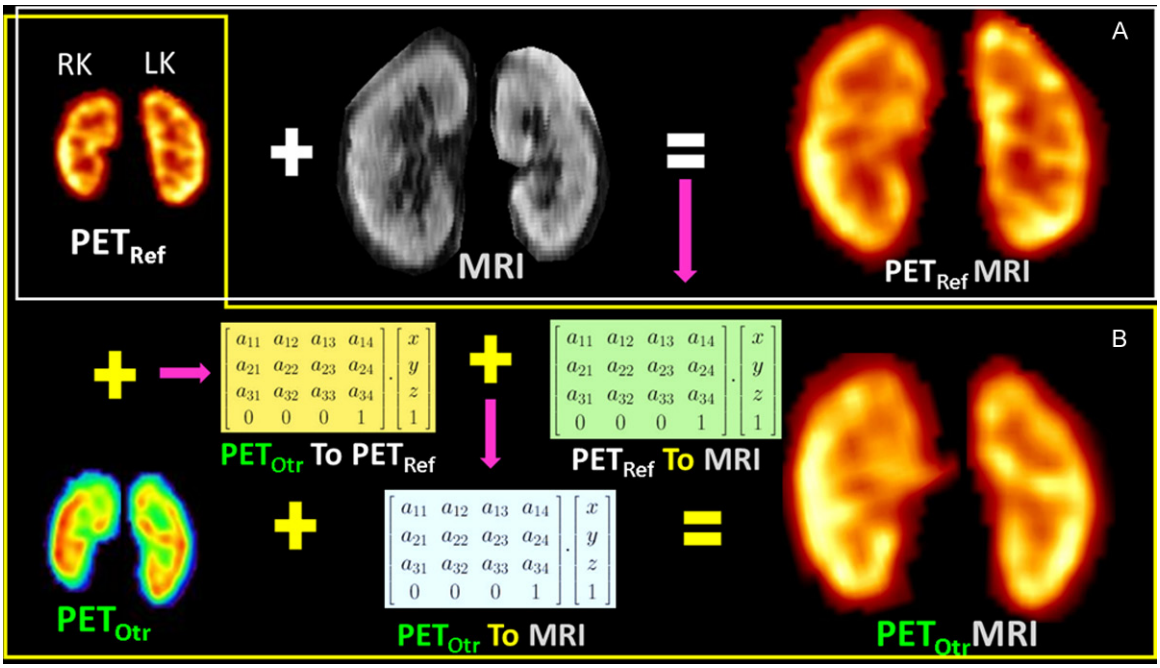

Figure 3. A. PET image was directly normalized to the template (MR image), where both PET_{Ref} and MR images were from the same subject (reference subject). B. PET image was normalized to the template through an intermediate PET space registration process, where PET_{Otr} images of other subjects were registered to the reference subject's PET_{Ref} image, then the transformation matrix obtained from this process (PET_{Otr} To PET_{Ref}) was concatenated with the transformation matrix obtained from process-A (PET_{Ref} To MR) and finally the resultant transformation matrix (PET_{otr} To MR) was applied on PET_{Otr} image of other subjects to get the normalized image.

plot has given us an overall picture of the difference between HC and CRF in terms of parameter mean value calculated over the whole kidney. But it does not provide us the regional significant differences between these groups. To obtain such significance within the kidney area the statistical map of K_1, k_2 and V_a parameters were created (**Figure 6**), which represents how HC and CRF are significantly different from each other locally. Statistical significance was determined using voxel-by-voxel t-test analysis among the parameter values at each voxel for the HC group to those for the CRF group. The orthogonal and 3D view shows the significant increase in K_1, k_2 and V_a parameter for HC compared to those for CRF within several areas of both kidney. Since the clearance parameter, k_2 provides an image with reasonable accuracy and quality [5], this article recommends using the statistical map of the k_2 parameter for precise comparison.

Discussion

In terms of computational performance conventionally used region of interest (ROI) based nonlinear least-squares fitting (NLF) technique [20-22] is extremely difficult to generate a parametric image by calculating parameter values for each voxel. To overcome this difficulty Koeppe et al. [23] introduced the BFM, where the nonlinear terms are first computed and the parameters of each voxel are linearly solved, making the estimation of the parameters rapid which makes BFM is an efficient method to generate blood flow kinetic parametric images. The BFM for generating local blood flow parametric image of kidney as well as other organs have been validated in several studies using PET [5, 8, 24, 25]. Since such a process of verification was already applied and presented in other literature [5], we did not validate it here.

The use of ^{15}O-water with this technique offers several advantages [4], such as its short half-life (2 min), which enables easily repeated scans. Other advantages are that ^{15}O-water is a metabolically inert tracer that is highly diffusible and consistent with the inherent function of the kidney and the synthesis of ^{15}O-labeled compounds is relatively easy. However, some disadvantage of this technique compared with other techniques is that because of the short half-life, $H_2{}^{15}O$ production requires an on-site

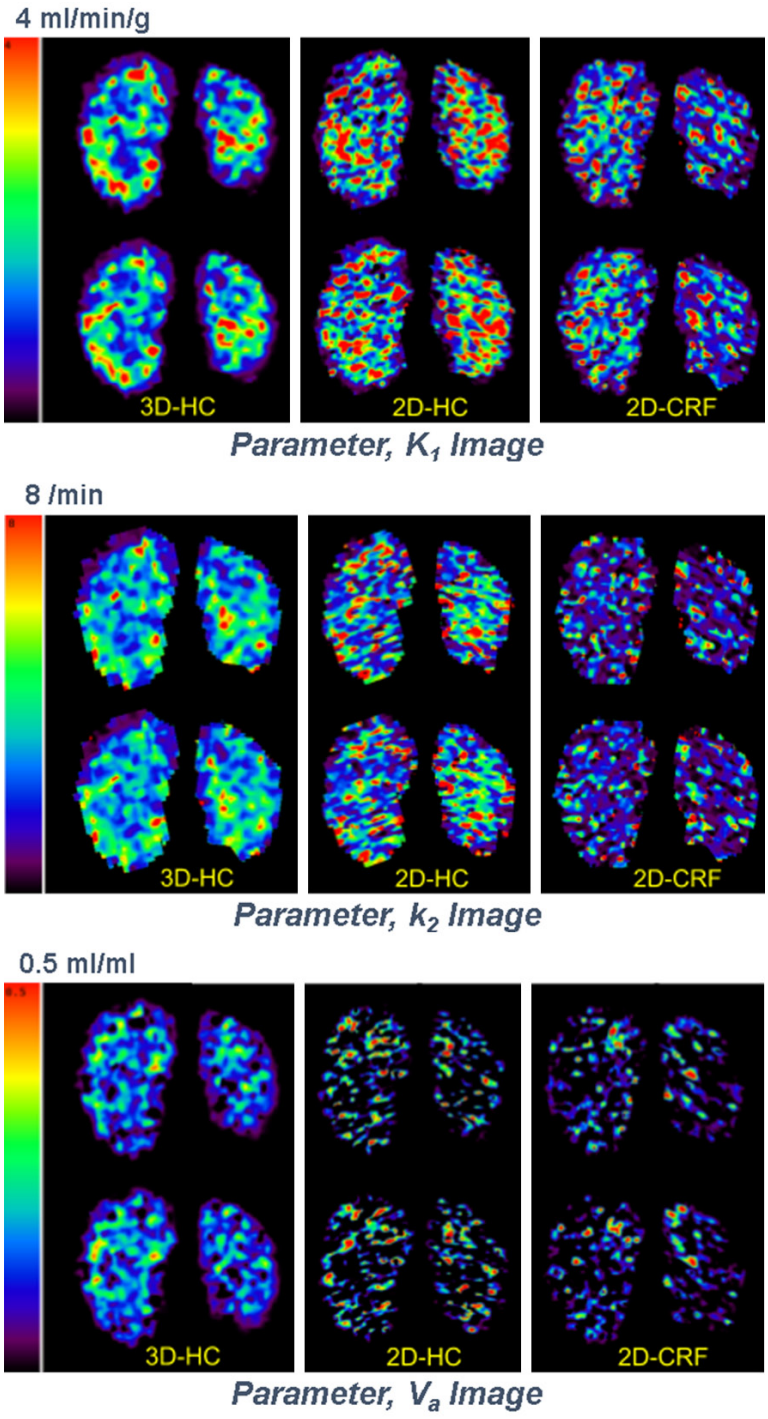

Figure 4. Parametric images of volumetrically normalized kidney generated through BFM.

cyclotron and the small distribution volume of ^{15}O-water in the kidney, the tracer rapidly disappears. Consequently, the image quality is limited making the computation of kinetic parameters at a voxel level by this technique difficult [8]. Since the workplace is facilitated with an on-site cyclotron and 3D PET scanner produced better quality image compared to 2D PET scanner, we were able to prevail over the problems associated with ^{15}O imaging. Additionally, better quality 3D PET image was used as an intermediate template for volumetric normalization process (**Figure 3B**). The image quality also has an impact on the image-driven input function which results in an underestimation in the quantification.

Essential parts for group-level image statistics are the volumetric normalization of the PET images and precise prototyping of the volumes of interest (VOIs). For accurate quantification of PET images dedicated individual MRI-PET precise co registration and manual demarcation of the VOIs are necessary. Since this process is lengthy and it could be difficult by inter- and intra-operator variability, template based volumetric normalization and delineation of VOIs is very attractive to standardize the analysis. However, one must be cautious for choosing a specific template as various templates are categorized by differences in performance and they might cause the introduction of inaccuracies and under- or overestimations in the quantification [32]. We have used one HC subject's kidney MR image as our template which restrains us for achieving perfect volumetric normalized images especially for CRF subjects with affine transformation. Due to the limitation of the experimental resource, we could not aim for obtaining perfect registration rather we wanted to establish a method by which statistically significant differences between HC and CRF groups in terms of kidney blood flow kinetic parameters can be observed

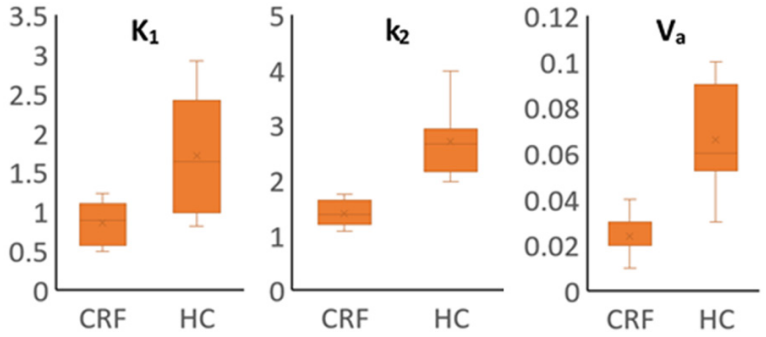

Figure 5. Box plot of HC and CRF in terms of parameter mean value calculated over the whole kidney.

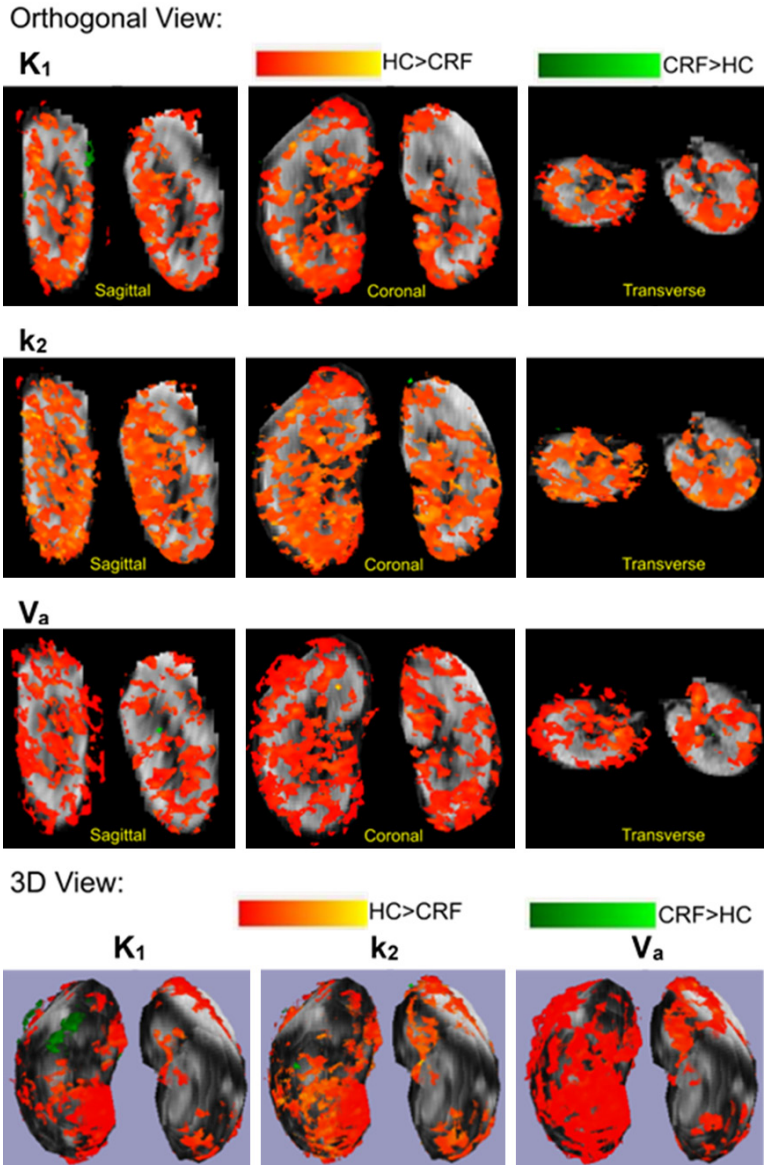

Figure 6. Orthogonal and 3D view of statistical map of K_1, k_2 and V_a parameters. The statistical t-map generated using threshold-free cluster enhancement (TFCE) in permutation methods without family-wise error rate (FWER) correction. Colored pixels represent kidney areas that showed group averaged K_1, k_2 and V_a parameter values where HC significantly different from CRF. Images were produced using FSLeyes software by overlaying statistical images of HC>CRF (Red-Yellow) and CRF>HC (Green) on the MR template.

locally and that is evident as an outcome of this method (**Figure 6**). However, a perfect registration along with template optimization technique [33] could enhance the accuracy of the method. Having only one subject MRI for this study is a limitation for obtaining an optimized template. Furthermore, better registration can be achieved by choosing a high-precision nonlinear registration method [33].

We incorporated threshold-free cluster enhancement (TFCE) in the randomize method because TFCE does indeed provide not just improved sensitivity, but richer and more interpretable output than standard voxel by voxel method and other cluster-based methods [29, 34]. Additionally, permutation in combination with TFCE, providing accurate type 1 FWER. In the case of small sample sizes (*N*=10, 25 trials), the permutation technique is preferable as it offers better control over the type 1 FWER [35]. However, due to small sample size (10 scans), which require 210 permutation or iterations for the exhaustive test of t-test, performing FWER correction would be too liberal because 600 to 800 iterations are necessary to achieve the nominal FWER, irrespective of the technique considered [35].

It is expected to increase the incidence of kidney diseases, such as atherosclerosis, diabetic nephropathy, and cancer due to the increasing age of the general population [36]. Without developing novel molecular imaging techniques, it would be challenging for the successful management of these diseases. Since PET permits quantitative imaging of the kidney, it has enormous potentiality in kidney imaging not only to measure blood flow but also in various types of functional and molecular imaging and in the development of molecular tracers for kidney imaging [2]. Numerous MRI techniques like cine phase-contrast MRI, arterial spin labeling (ASL) MRI, Blood oxygen level-dependent (BOLD) MRI are also very appealing in functional kidney imaging [1]. These potential new approaches are, at best, in an experimental stage [2]. Several volumetric normalizations and image statistics robust applications namely, FSL, statistical parametric map (SPM), three-dimensional stereotactic surface projections (3D-SSP), etc. are successfully being used in clinical and basic research for functional and molecular brain imaging that usages PET, MRI, SPECT. Using FSL, we have shown that these applications can easily be used for functional and molecular imaging of kidney, which can be implemented for various types of kidney mapping studies, group comparison and even for automation in disease diagnosis.

Conclusion

Since statistical mapping of the brain has become an essential tool for functional and molecular imaging in brain research and clinical application, it is apparent from this study that, statistical mapping of kidney could play a significant role in the success of renal functional and molecular imaging research and for the better diagnosis of kidney diseases that usage PET, MRI, CT and SPECT. However, a bigger sample size would result in a better outcome. This article also suggests that such kind of image statistics can be performed for functional and molecular images of other organs like the lung, the liver and even for the whole body.

Acknowledgements

This study was supported by Grants-in-Aid for Scientific Research No. 25670405 and No. 17H04118 from the Ministry of Education, Culture, Sports, Science and Technology (NEXT), Japanese Government. This study was approved by the Ethics Committee of the Tohoku University Hospital (No. 2010-329).

Written informed consent was obtained from all subjects after a complete description of the study had been made.

Disclosure of conflict of interest

None.

Address correspondence to: Hiroshi Watabe, Division of Radiation Protection and Safety Control, Cyclotron and Radioisotope Center (CYRIC), Graduate School of Biomedical Engineering, Tohoku University, Aoba-6-3, Aramaki, Aoba-ku, Sendai-shi, Miyagi-ken 980-0845, Japan. Tel: 022-795-7803; Fax: 022-795-7809; E-mail: watabe@cyric.tohoku.ac.jp

References

[1] Schneider AG, Goodwin MD, Bellomo R. Measurement of kidney perfusion in critically ill patients. Crit Care 2013; 17: 220.

[2] Szabo Z, Xia J, Mathews WB, Brown PR. Future Direction of Renal Positron Emission Tomography. Semin Nucl Med 2006; 36: 36-50.

[3] Thurman JM and Gueler F. Recent advances in renal imaging [version 1; peer review: 3 approved]. F1000Research 2018, 7(F1000 Faculty Rev):1867.

[4] Alpert NM, Rabito CA, Correia DJ, Babich JW, Littman BH, Tompkins RG, Rubin NT, Rubin RH, Fischman AJ. Mapping of local renal blood flow with PET and H(2)(15)O. J Nucl Med 2002; 43: 470-5.

[5] Kudomi N, Koivuviita N, Liukko KE, Oikonen VJ, Tolvanen T, Iida H, Tertti R, Metsärinne K, Iozzo P, Nuutila P. Parametric renal blood flow imaging using [^{15}O]H_2O and PET. Eur J Nucl Med Mol Imaging 2009; 36: 683-91.

[6] Kero T, Nordström J, Harms HJ, Sörensen J, Ahlström H, Lubberink M. Quantitative myocardial blood flow imaging with integrated time-of-flight PET-MR. EJNMMI Phys 2017; 4: 1.

[7] van der Veldt AA, Hendrikse NH, Harms HJ, Comans EF, Postmus PE, Smit EF, Lammertsma AA, Lubberink M. Quantitative parametric perfusion images using ^{15}O-labeled water and a clinical PET/CT scanner: test-retest variability in lung cancer. J Nucl Med 2010; 51: 1684-1690.

[8] Watabe H, Jino H, Kawachi N, Teramoto N, Hayashi T, Ohta Y, Iida H. Parametric imaging of myocardial blood flow with ^{15}O-water and PET using the basis function method. J Nucl Med 2005; 46: 1219-24.

[9] Crivello F, Schormann T, Tzourio-Mazoyer N, Roland PE, Zilles K, Mazoyer BM. Comparison of spatial normalization procedures and their impact on functional maps. Hum Brain Mapp 2002; 16: 228-50.
[10] Rocha ET, Buchpiguel CA, Nitrini R, Tazima S, Peres SV, Busatto Filho G. Diagnosis of regional cerebral blood flow abnormalities using SPECT: agreement between individualized statistical parametric maps and visual inspection by nuclear medicine physicians with different levels of expertise in nuclear neurology. Clinics (Sao Paulo) 2009; 64: 1145-53.
[11] Ohta Y, Nariai T, Ishii K, Ishiwata K, Mishina M, Senda M, Hirakawa K, Ohno K. Voxel- and ROI-based statistical analyses of PET parameters for guidance in the surgical treatment of intractable mesial temporal lobe epilepsy. Ann Nucl Med 2008; 22: 495-503.
[12] Kono AK, Ishii K, Sofue K, Miyamoto N, Sakamoto S, Mori E. Fully automatic differential diagnosis system for dementia with Lewy bodies and Alzheimer's disease using FDG-PET and 3D-SSP. Eur J Nucl Med Mol Imaging 2007; 34: 1490-7.
[13] Ishii K, Kono AK, Sasaki H, Miyamoto N, Fukuda T, Sakamoto S, Mori E. Fully automatic diagnostic system for early- and late-onset mild Alzheimer's disease using FDG PET and 3D-SSP. Eur J Nucl Med Mol Imaging 2006; 33: 575-83.
[14] Slomka PJ, Dey D, Sitek A, Motwani M, Berman DS, Germano G. Cardiac imaging: working towards fully-automated machine analysis & inter-pretation. Expert Rev Med Devices 2017; 14: 197-212.
[15] Fujiwara T, Watanuki S, Yamamoto S, Miyake M, Seo S, Itoh M, Ishii K, Orihara H, Fukuda H, Satoh T, Kitamura K, Tanaka K, Takahashi S. Performance evaluation of a large axial field-of-view PET scanner: SET-2400W. Ann Nucl Med 1997; 3: 307-313.
[16] Matsumoto K, Kitamura K, Mizuta T, Tanaka K, Yamamoto S, Sakamoto S, Nakamoto Y, Amano M, Murase K, Senda M. Performance charac-teristics of a new 3-dimensional continuous-emission and spiral-transmission high-sensitivity and high-resolution PET camera evaluated with the NEMA NU 2-2001 standard. J Nucl Med 2006; 47: 83-90.
[17] Tanaka E, Kudo H. Subset-dependent relaxation in block-iterative algorithms for image reconstruction in emission tomography. Phys Med Biol 2003; 48: 1405-22.
[18] Tanaka E and Kudo H. Optimal relaxation parameters of DRAMA (dynamic RAMLA) aiming at one-pass image reconstruction for 3D-PET. Phys Med Biol 2010; 55: 2917-39.
[19] Hudson HM, Larkin RS. Accelerated image reconstruction using ordered subsets of projection data. IEEE Trans Med Imaging 1994; 13: 601-609.
[20] Nitzsche EU, Choi Y, Killion D, Hoh CK, Hawkins RA, Rosenthal JT, Buxton DB, Huang SC, Phelps ME, Schelbert HR. Quantification and parametric imaging of renal cortical blood flow in vivo based on Patlak graphical analysis. Kidney Int 1993; 44: 985-96.
[21] Juillard L, Janier MF, Fouque D, Lionnet M, Le Bars D, Cinotti L, Barthez P, Gharib C, Laville M. Renal blood flow measurement by positron emission tomography using ^{15}O-labeled water. Kidney Int 2000; 57: 2511-18.
[22] Juillard L, Janier MF, Fouque D, Cinotti L, Maakel N, Le Bars D, Barthez PY, Pozet N, Laville M. Dynamic renal blood flow measurement by positron emission tomography in patients with CRF. Am J Kidney Dis 2002; 40: 947-54.
[23] Koeppe RA, Holden JE, Ip WR. Performance comparison of parameter estimation techniques for the quantitation of local cerebral blood flow by dynamic positron computed tomography. J Cereb Blood Flow Metab 1985; 5: 224-34.
[24] Gunn RN, Lammertsma AA, Hume SP, Cunningham VJ. Parametric imaging of ligand-receptor binding in PET using a simplified reference region model. Neuroimage 1997; 6: 279-87.
[25] Boellaard R, Knaapen P, Rijbroek A, Luurtsema GJ, Lammertsma AA. Evaluation of basis function and linear least squares methods for generating parametric blood flow images using ^{15}O-water and positron emission tomography. Mol Imaging Biol 2005; 7: 273-85.
[26] Watabe H, Channing MA, Riddell C, Jousse F, Libutti SK, Carrasquillo JA, Bacharach SL, Carson RE. Noninvasive estimation of the aorta input function for measurement of tumor blood flow with [150] water. IEEE Trans Med Imaging 2001; 20: 164-174.
[27] Jenkinson M and Smith S. A global optimisation method for robust affine registration of brain images. Med Image Anal 2001; 5: 143-56.
[28] Jenkinson M, Bannister PR, Brady JM and Smith SM. Improved optimisation for the robust and accurate linear registration and motion correction of brain images. NeuroImage 2002; 17: 825-841.
[29] Smith SM, Nichols TE. Threshold-free cluster enhancement: addressing problems of smoothing, threshold dependence and localisation in cluster inference. NeuroImage 2009; 44: 83-98.
[30] Salimi-Khorshidi G, Smith SM, Nichols TE. Adjusting the effect of nonstationarity in cluster-based and TFCE inference. NeuroImage 2011; 54: 2006-2019.

[31] Winkler AM, Ridgway GR, Webster MA, Smith SM, Nichols TE. Permutation inference for the general linear model. NeuroImage 2014; 92: 381-397.
[32] Bertoglio D, Verhaeghe J, Kosten L, Thomae D, Van der Linden A, Stroobants S, Wityak J, Dominguez C, Mrzljak L, Staelens S. MR-based spatial normalization improves [18 F]MNI-659 PET regional quantification and detectability of disease effect in the Q175 mouse model of Huntington's disease. PLoS One 2018; 13: e0206613.
[33] Wang M, Li P, Liu F. Multi-atlas active contour segmentation method using template optimization algorithm. BMC Med Imaging 2019; 19: 42.
[34] Roiser JP, Linden DE, Gorno-Tempinin ML, Moran RJ, Dickerson BC, Grafton ST. Minimum statistical standards for submissions to Neuroimage: Clinical. Neuroimage Clin 2016; 12: 1045-1047.
[35] Pernet CR, Latinus M, Nichols TE, Rousselet GA. Cluster-based computational methods for mass univariate analyses of event-related brain potentials/fields: a simulation study. J Neurosci Methods 2015; 250: 85-93.
[36] Szabo Z, Alachkar N, Xia JS, Mathews WB, Rabb H. Molecular Imaging of the Kidneys. Semin Nucl Med 2011; 41: 20-8.